Article

Process-induced extracellular matrix alterations affect the mechanisms of soft tissue repair and regeneration

Journal of Tissue Engineering
4: 2041731413505305

DOI: 10.1177/2041731413505305
tej.sagepub.com
SAGE

Wendell Q Sun[1,2], Hui Xu[2], Maryellen Sandor[2] and Jared Lombardi[2]

Abstract

Extracellular matrices derived from animal tissues for human tissue repairs are processed by various methods of physical, chemical, or enzymatic decellularization, viral inactivation, and terminal sterilization. The mechanisms of action in tissue repair vary among bioscaffolds and are suggested to be associated with process-induced extracellular matrix modifications. We compared three non-cross-linked, commercially available extracellular matrix scaffolds (Strattice, Veritas, and XenMatrix), and correlated extracellular matrix alterations to in vivo biological responses upon implantation in non-human primates. Structural evaluation showed significant differences in retaining native tissue extracellular matrix histology and ultrastructural features among bioscaffolds. Tissue processing may cause both the condensation of collagen fibers and fragmentation or separation of collagen bundles. Calorimetric analysis showed significant differences in the stability of bioscaffolds. The intrinsic denaturation temperature was measured to be 51°C, 38°C, and 44°C for Strattice, Veritas, and XenMatrix, respectively, demonstrating more extracellular matrix modifications in the Veritas and XenMatrix scaffolds. Consequently, the susceptibility to collagenase degradation was increased in Veritas and XenMatrix when compared to their respective source tissues. Using a non-human primate model, three bioscaffolds were found to elicit different biological responses, have distinct mechanisms of action, and yield various outcomes of tissue repair. Strattice permitted cell repopulation and was remodeled over 6 months. Veritas was unstable at body temperature, resulting in rapid absorption with moderate inflammation. XenMatrix caused severe inflammation and sustained immune reactions. This study demonstrates that extracellular matrix alterations significantly affect biological responses in soft tissue repair and regeneration. The data offer useful insights into the rational design of extracellular matrix products and bioscaffolds of tissue engineering.

Keywords

Biological scaffold, extracellular matrix, decellularization, matrix remodeling, soft tissue regeneration, bovine pericardium, porcine dermis, tissue engineering

Introduction

One of the strategies to repair and regenerate damaged or diseased soft tissues is extracellular matrix (ECM)-induced in situ tissue formation that leads to the restoration and improvement of functions of affected tissues and organs. The pathway involves ECM preparation, implantation, host cell repopulation, revascularization, and remodeling of ECM scaffold. ECM scaffolds contain many structural proteins with proper extracellular architecture, and signaling molecules such as fibronectin, integrins, laminin, and sequestered growth factors. The implanted ECM scaffold provides biomechanical support and can elicit new tissue formation by interacting with host cells to modulate cell behaviors such as adhesion, migration, proliferation, and differentiation, as well as to modulate inflammatory responses and remodeling of ECM scaffolds.[1–6] Presently, about 30 tissue-derived scaffold products have received approval from United States and European regulatory

[1]Institute of Biomedical Technology, School of Medical Instruments and Food Engineering, University of Shanghai for Science and Technology, Shanghai, China
[2]LifeCell Corporation, Bridgewater, NJ, USA

Corresponding author:
Wendell Q Sun, School of Medical Instruments and Food Engineering, University of Shanghai for Science and Technology, Shanghai 200093, China.
Email: Wendell.q.sun@gmail.com

authorities, and are marketed for various clinical applications in tissue repair and regeneration,[3,7–9] with 2011 US sales alone exceeding US$1 billion.[10] These scaffolds are derived from a variety of human and mammalian tissues, including blood vessel, heart valve, ligament, nerve, skin, small intestinal submucosa, forestomach, pericardium, peritoneum, tendons, and urinary bladder. ECM-based scaffolds are the first wave of commercially available products for tissue engineering and regenerative medicine, and have achieved considerable success satisfying unmet clinical needs. This approach has been used to reconstruct and to repair increasingly more complex tissues and organs in human patients,[11,12] and may be a promising platform for engineering whole functional organs by using in vitro recelluarization and matrix remodeling with autologous stem cells or differentiated cells.[13]

When an ECM scaffold is derived from donated human or other mammalian tissues, the native ECM is subjected to biochemical and structural alterations during processing that involves chemical, enzymatic, or physical decellularization, antigenicity reduction treatment, viral inactivation, and terminal sterilization. Different processing methods are known to yield ECM materials with different structural and biological properties.[9,14–18] Preclinical and clinical evidences demonstrate that not all biologically derived scaffolds are equal and that host responses in tissue regeneration vary among scaffold products.[8,19–26] The variation of performance in tissue repair and regeneration among scaffolds is presumably due to different tissue sources, the presence of undesirable cellular and matrix elements, and matrix damage or modifications upon tissue processing.[2,7,9,15,20,22,23,26–28] However, there are no generally accepted performance specifications for biological scaffolds, and little information is available about ECM modifications among commercially available scaffold products. How the process-induced ECM modifications affect the mechanisms of action in tissue repair remains poorly understood.

To gain insight into the rational design of tissue engineering scaffolds, this study has examined ECM modifications in three non-cross-linked, commercially available scaffolds (Strattice™ reconstructive tissue matrix, Veritas® collagen matrix, and XenMatrix™ surgical graft). It aims to correlate the comparative differences in ECM modifications among three scaffolds to biological responses in tissue repair and regeneration after implantation in a primate model. The comparative investigation of commercially available scaffolds may offer valuable biochemical and structural insights into the rational design of tissue engineering scaffolds.

Material and methods

Ethics statements

A part of the research project involves the use of non-human primate subjects. The non-human primate study was performed in strict compliance with the recommendations in the Guide for the Care and Use of Laboratory Animals of the National Institutes of Health, and all appropriate parts of the Animal Welfare Act of 1966 (P.L. 89-544), as amended by the Animal Welfare Act of 1970 (P.L. 91-579) and the 1976 amendments to the Animal Welfare Act (P.L. 94-279)—9 Code of Federal Regulations (CFR) Chapter I (1 January 1998 edition) as well as the *International Guiding Principles for Biomedical Research Involving Animals* developed by the Council for International Organizations of Medical Sciences and the following guidelines for animal welfare. The study protocol was reviewed and approved by the Institutional Animal Care and Use Committee (IACUC), the Behavioral Sciences Foundation (St Kitts, Eastern Caribbean). The research facility of the Behavioral Sciences Foundation is accredited by the Canadian Council for Animal Care and has a Public Health Service (PHS)-approved Animal Welfare Assurance (A5535-01) issued by the Office of Laboratory Animal Welfare (OLAW).

Tissue-based biological scaffolds

Strattice reconstructive tissue matrix (LifeCell Corporation, Branchburg, NJ) is derived from porcine dermis with a process that removes cellular elements and reduces α-gal epitope in ECM via enzymatic cleavage. Viral reduction and e-beam irradiation are applied to yield a sterile scaffold that retains structural and biochemical integrity of porcine dermis ECM.[22,29] Veritas collagen matrix (Synovis Life Technologies, St Paul, MN) is derived from bovine pericardium. Pericardium is decellularized and exposed to 1.0 N sodium hydroxide to eliminate bovine spongiform encephalopathy (BSE) transmission. The decellularized pericardium is then treated with propylene oxide for capping primary amine groups to reduce immunogenicity. Veritas is terminally sterilized by e-beam irradiation.[30–32] XenMatrix surgical graft (Davol, Inc., Warwick, RI) is also derived from porcine dermis, which is treated by a proprietary processing technology to achieve an open matrix structure designed to encourage cell repopulation and minimize encapsulation by fibrotic tissue.[33] The XenMatrix process involves (a) freezing, thawing, and bleaching of porcine dermis to loosen the collagen matrix; (b) removing non-collagenous elements; and (c) treating with sodium hydroxide solution and hydrogen peroxide solution to improve biocompatibility.[34] XenMatrix graft is sterilized by e-beam irradiation. All three products are packaged in the hydrated state, and labeled as being non-cross-linked and stable for room temperature storage. These scaffolds are increasingly utilized to support soft tissue regeneration, including applications in hernia repairs, and urological, gynecological, and breast reconstruction surgeries.[8,35–37]

Minimally processed ECM materials

To evaluate the extent of ECM modifications in commercially available scaffolds, minimally processed porcine dermis

ECM (pd-ECM) and bovine pericardium ECM (bp-ECM) were derived from freshly slaughtered animals to serve as controls. Porcine skin from 6-month-old animals and bovine pericardium from 18- to 24-month-old animals were cleaned manually to remove hairs, epidermis, and adipose tissue. Isolated dermis (~1.0 mm thick) and pericardium (~0.4–0.7 mm thick) were aseptically decellularized in 2% (w/v) sodium deoxycholate in 20 mM 4-(2-hydroxyethyl)-1-piperazineethanesulfonic acid (HEPES) (pH 8.0) containing 10 mM ethylenediaminetetraacetic acid (EDTA). Decellularization was carried out with gentle agitation for 8 h at 22°C–24°C, and decellularized ECMs were washed in Dulbecco's phosphate-buffered saline (PBS; pH 7.2) three times over a period of 18 h. The minimally processed tissue ECMs were temporarily stored in PBS at 4°C, and were used for testing within a week.

Histological and scanning electron microscopic evaluation

For histological analysis, samples of ECM materials were rinsed in 0.9% saline for 1 h before fixation in 10% buffered formalin solution. Samples were routinely processed through dehydration, embedment in paraffin, and sectioning. Tissue slices were stained with hematoxylin-eosin (H&E) stain. For scanning electron microscope (SEM) evaluation, tissue samples were fixed in 2% glutaraldehyde, cut to the desired size, and dehydrated through a series of ethanol solutions with increasing concentrations from 50% to 100%. Specimens in 100% ethanol were gradually changed to 100% hexamethyldisilazane for drying. Dried specimens were mounted and coated with gold palladium under vacuum (<8 Pa) for 120 s. The microstructures of samples were viewed, and micrographs were captured using a desktop SEM (NeoScope JCM-5000; Jeol Ltd, Tokyo, Japan) at 10 kV.

Calorimetric analysis

Samples of ECM materials were rinsed in Dulbecco's PBS (pH 7.4). Samples (25–30 mg) were hermetically sealed in aluminum crucibles. Thermograms were recorded using differential scanning calorimeter (Model Q2000; TA Instruments, New Castle, DE) from 2°C to 125°C at various heating rates between 0.02°C/min and 50°C/min. After calorimetric measurement, small holes were punched on sealed crucibles with a pin, and the dry mass of samples was measured after dehydration between 105°C and 110°C under vacuum overnight. Thermograms were analyzed using the software Universal Analysis 2000 (version 4.5) to determine the onset temperature (T_d) and enthalpy (ΔH) of collagen denaturation.

Collagenase susceptibility assay

The susceptibility of ECM materials to type I collagenase (Sigma–Aldrich, St Louis, MO) was tested at 37°C in vitro. Samples were rinsed in 0.9% saline, 60–80 mg material was placed in 2.0-mL Eppendorf tubes, and 1.5 mL of pre-warmed 10 mM Tris-HCl buffer containing 2 mM $CaCl_2$ (pH 7.5) was added to each sample. Collagenase was added to the sample in a final enzymic activity of 100 units/mL for digestion at 37°C for up to 16 h. After digestion, samples were centrifuged, washed with distilled water, and freeze-dried. The resistance of tissue matrix to collagenase digestion was determined according to the dry mass of remaining tissue.

In vivo biological response study with non-human primates

The study was performed in strict compliance with the recommendations in the Guide for the Care and Use of Laboratory Animals of the National Institutes of Health and other appropriated laws, as listed in the ethics statement above. The surgical procedure of abdominal wall repair according to Xu et al.,[21] and the study protocol were approved by the IACUC, the Behavioral Sciences Foundation (St Kitts, Eastern Caribbean). All procedures used in this study, including surgical procedure, housing conditions, feeding regimens, and environmental enrichment, have been designed to alleviate suffering and to avoid discomfort, distress, and pain to the animals. Monkeys were housed at the test facility in a way such that they maintained visual contact with other monkeys at all times, and kept outdoors in individual American Association for Accreditation of Laboratory Animal Care (AAALAC)-approved cages, protected from weather extremes and subject to the normal temperature and humidity levels to which the monkeys were accustomed in order to decrease external stress factors. They were fed with 20% Harlan 2050 (Harlan Laboratories, Indianopolis, IN) Teklad Global 20% Protein Primate Diet supplemented with fresh fruits and vegetables. Water was provided ad libitum via water bottles. Cages were cleaned and maintained on a daily basis per standard procedure at the animal care facility. The monkeys were monitored by the technical staff for any conditions requiring possible veterinary care. Animals selected for surgery received supplements for enrichment such as produce treats and bamboo branches. Tactile and sensory enrichment was provided in the form of puzzle feeders, which rotated around the colony. Any aspects of this study that might cause more than momentary or slight pain or distress to the animals was performed with appropriate sedatives, analgesics, or anesthetics. Animals that experienced severe or chronic pain or distress that could not be relieved were painlessly euthanized as deemed appropriate by the test facility's veterinarian. Additional detailed information has been provided as supplemental support information.

Adult male vervet monkeys (*Chlorocebus aethiops*), 3–6 kg, were screened for general health, and quarantined for 2 weeks before surgery. The monkeys were fasted for 24 h prior to the surgical procedure, and each animal was given an injection of ketamine HCl 40–60 mg intramuscularly (IM) as a pre-anesthetic to allow the technician to

safely handle the monkey prior to transportation to the procedure room. Each monkey received an injection of cefazolin sodium 125 mg IM (antibiotics) on the day of surgery. An intravenous (IV) catheter was placed in the monkey in order to provide access for IV fluids, which was maintained at a slow drip rate to keep the IV catheter patent and to assist flushing the line following IV injections. Just prior to the final preparation of the surgical site, the animal was given a combination of ketamine (10 mg/kg) and xylazine (1 mg/kg) IM. Additional ketamine/xylazine was given as needed throughout the procedure to maintain proper levels of anesthesia. For surgical implantation of a test material, a 3 cm × 7 cm full-thickness defect was created in the abdominal wall by removing the fascia, rectus muscle, and peritoneum. The defect was repaired with a test scaffold by tissue approximation to the defect edge and fixation using 3–0 polypropylene sutures. The area was draped using sterile drapes. Following the procedure, the monkeys were allowed to recover under the observation of a staff member, and were treated as necessary in order to assure a complete and uncomplicated recovery. Monkeys also received the analgesic drug flunixin meglumine at approximately 2.0–5.0 mg/kg IM or buprenorphine at 0.01 mg/kg subcutaneously (SC) or IM either prior to the surgical procedure or immediately following surgery. Additional administration was allowed twice daily for 3 days or longer depending on signs of pain as determined by the facility veterinarian.

Strattice, Veritas, and XenMatrix were investigated at 1-, 3-, and 6-month time points, with three animals euthanized for each test material per time point. The gross assessment of repairs was made for herniation or bulging in animals over the course of implantation. On the day of termination, the monkeys were given an injection of ketamine HCl 40–60 mg IM to allow the technician to safely handle the monkey prior to transportation to the necropsy room. Additional ketamine was given as needed throughout the procedure to maintain proper levels of anesthesia while drawing blood and performing the pre-explantation physical exam. After animals were sacrificed, explanted grafts were examined for scaffold integration with adjacent host tissue, and the possible presence of graft defect or hardening. The sizes of explanted scaffolds were measured, and percentage of graft contraction after implantation was calculated. Explanted samples were fixed in 10% buffered formalin solution for histological analysis as described earlier. Tissue sections from the center and interface of each graft material were stained with H&E. Histological evaluation was done by blinded assessment for host cell infiltration, revascularization, inflammatory response, and collagen remodeling.

Antibody determination after material implantation

Blood samples were taken after implantation at various time points up to 6 months. Serum was tested for the presence of elevated antibodies reacting to implanted scaffolds (immunoglobulin G, IgG). Pre-implant samples were rinsed with 0.9% saline, freeze-dried, and micronized using a cryo-mill with liquid nitrogen. Micronized tissue powder was suspended in PBS, which was used to coat Immulon 96-well polystyrene microtiter plates (Thermo Fisher Scientific, Waltham, MA) by air-drying overnight. Serial dilutions of serum samples were incubated in the coated microtiter wells for 2 h. Plates were then washed and incubated for 1 h with goat anti-human IgG conjugated to alkaline phosphatase. Plates were rinsed and incubated with *p*-nitrophenyl phosphate substrate for 1 h for detection. Reaction product was measured at 405 nm in a plate reader, and the increase in antibody titer was determined according to the serial dilution curve.

Results

Structural differences in scaffolds

The matrix structures of three scaffolds vary significantly (Figure 1). Both Strattice and XenMatrix are derived from porcine dermis with proprietary processing technologies. On histological examination as compared with unprocessed porcine dermis (supplemental Figure S1), the structural integrity of native dermis ECM is retained in Strattice with a uniform architecture of intact collagen bundle structures and the absence of cells. XenMatrix comprises an altered dermal matrix that shows structural dissimilarity from native dermal ECM. Collagen bundles in XenMatrix are fragmented and largely separated. The matrix of pericardium-derived Veritas has a diffuse appearance that lacks the well-defined structural features in unprocessed pericardial ECM. On SEM examination, micrographs reveal more microscopic structural differences among the three scaffolds (Figure 2). Strattice appears as a tightly intertwined and/or interwoven scaffold of collagen bundles, the fibrillar ultra-structures of which are preserved at fibril and fiber levels. Large pores over 50 μm are few between collagen bundles, and are mostly void spaces of blood vessels or removed hair follicles. XenMatrix does not show the architecture of porcine dermal ECM. Collagen fibrils and fibers in XenMatrix are fused together, leading to the complete loss of fibrillar ultra-structures of collagen bundles. Collagen bundles of XenMatrix are condensed, resulting in the formation of many large pores within the matrix. Veritas shows a very loose scaffold of collagen bundles, and large pores over 50 μm are abundant. The fibrillar ultra-structures of collagen bundles in Veritas are also preserved at fibril and fiber levels.

Differences in calorimetric characteristics

The DSC thermogram of fresh porcine dermis consists of multiple overlapping endothermic peaks between 20°C and

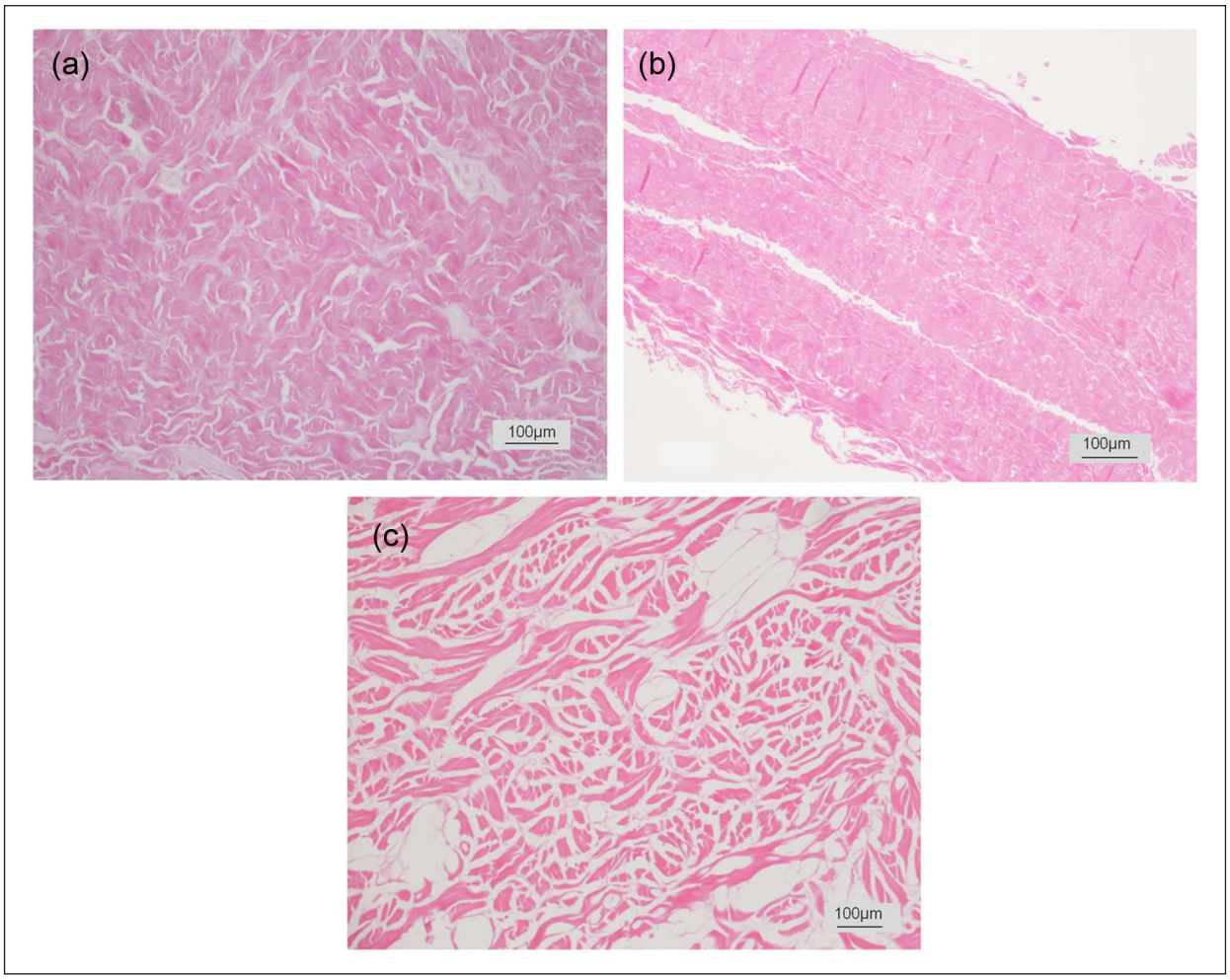

Figure 1. *Histological micrographs of bioscaffolds*. Histological micrographs of three commercially available bioscaffolds (cross sections with hematoxylin and eosin stain): (a) Strattice, (b) Veritas, and (c) XenMatrix.

120°C (Figure 3). Upon heating at a scan rate of 3°C/min, protein denaturation starts at 54.0°C ± 0.2°C, and the event ends when temperature reaches around 90°C, with a total enthalpic value of 54.8 ± 2.4 J/g (n = 9). The complex thermogram of unprocessed porcine dermis consists of three separate denaturation events (Peaks A, B, and C), which account for 16.7% ± 3.0%, 41.1% ± 4.8%, and 42.2% ± 4.0%, respectively (supplemental Figure S2). Peak A disappears after cell lysis and washing in saline or PBS. The pdECM retains Peaks B and C, without any change in their onset and peak temperatures. The DSC thermogram of fresh bovine pericardium starts at a much higher temperature, 63.0°C ± 0.5°C, with a smaller enthalpic value of 45.6 ± 4.4 J/g (n = 10) (Figure 3). It appears that the thermogram of bovine pericardium consists of only Peaks B and C between 20°C and 120°C, and Peak A in the lower temperature region is insignificant. The minimally processed bovine pericardial ECM has essentially the same DSC thermogram as fresh bovine pericardium (data not shown).

Commercially available scaffolds have calorimetric thermograms that are different from those of their respective unprocessed and/or minimally processed materials (Figure 4). Thermograms of these scaffolds consist of two denaturation peaks, one with a peak width of about 10°C followed by a very broad peak with a width about 40°C. For Strattice and XenMatrix, Peak A is no longer present in finished scaffolds. Peaks B and C at the higher temperature region are still retained in finished scaffolds; however, the changes in denaturation temperature and curve shape (as compared to unprocessed dermis and minimally processed dermis) have demonstrated ECM alterations upon tissue processing (Figures 3 and 4). Strattice has an onset denaturation temperature of 55.5°C ± 0.2°C, and an enthalpy of 56.6 ± 6.7 J/g (n = 5). The onset denaturation temperature of XenMatrix is decreased to a lower temperature (48.3°C ± 0.5°C, n = 6). There is no significant difference in enthalpy between Strattice and XenMatrix. The greatest change is observed in bovine pericardium-derived Veritas (Figures 3 and 4). The onset denaturation temperature of Veritas is decreased to 42.9°C ± 0.2°C, whereas the enthalpy is increased to 56.6 ± 5.1 J/g (n = 3).

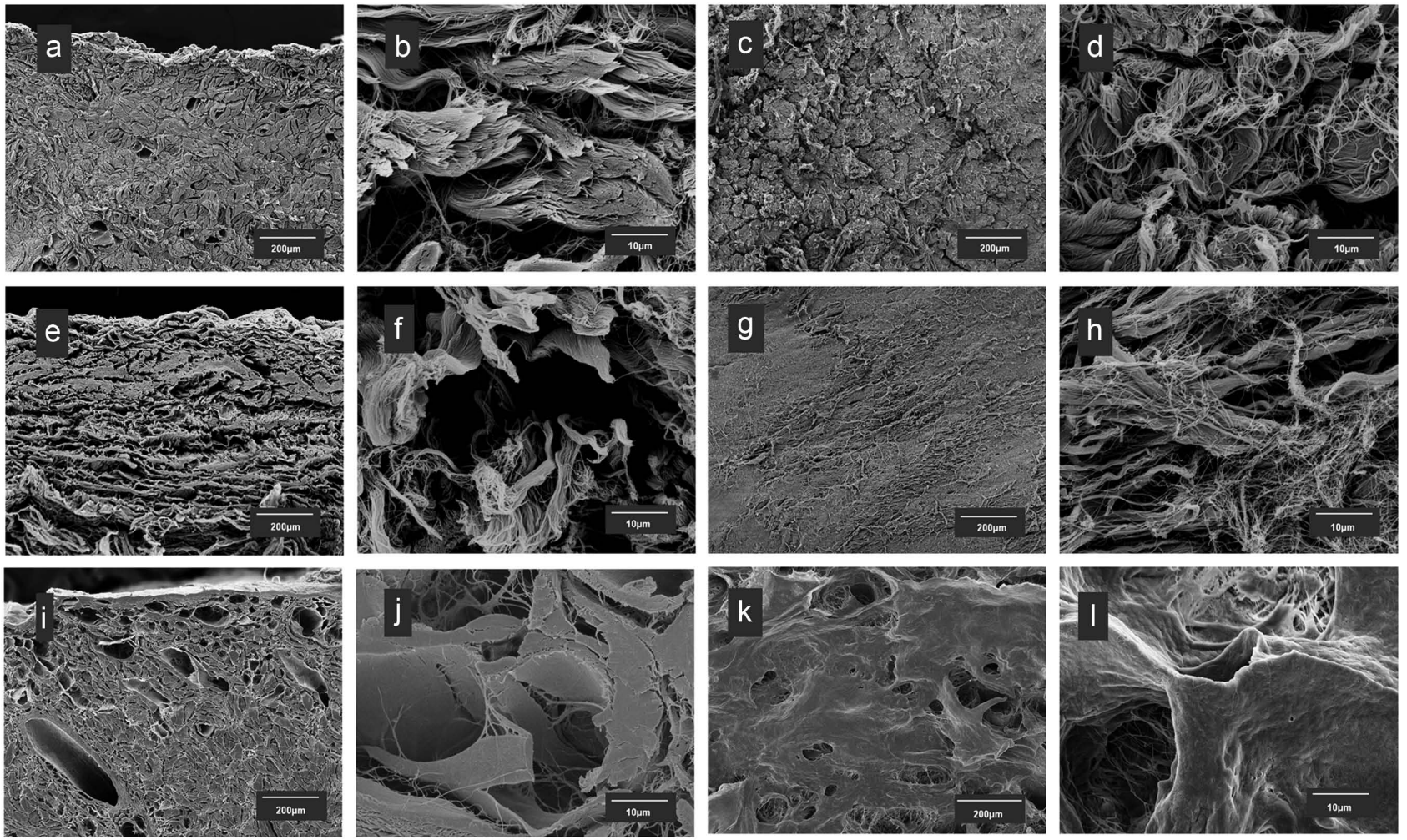

Figure 2. *Micro- and ultrastructural features of bioscaffolds.* Scanning electron micrographs of three commercially available bioscaffolds: (a–d) Strattice, (e–h): Veritas, and (i–l) XenMatrix. (a, b, e, f, i, and j) Cross sections and (c, d, g, h, k, and l) surface views.

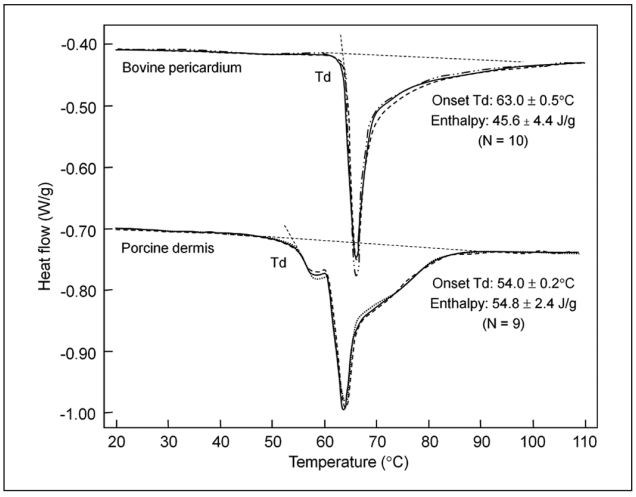

Figure 3. *Thermograms of unprocessed animal tissues.* Calorimetric thermograms of fresh bovine pericardium and porcine dermis at the scan rate of 3°C/min. Three independent test curves are superimposed for each material type. T_d denotes the onset denaturation temperature.

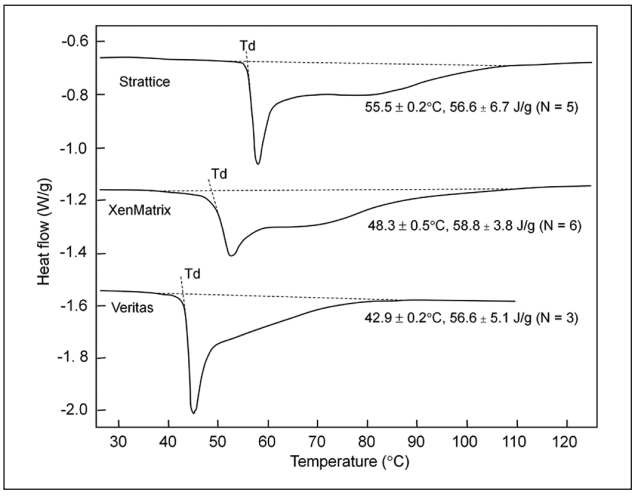

Figure 4. *Thermograms of bioscaffold denaturation.* Calorimetric thermograms of three bioscaffolds at the scan rate of 3°C/min. Note that significant modifications of extracellular matrices are observed in finished bioscaffold products when compared to unprocessed fresh tissues (see Figure 3).

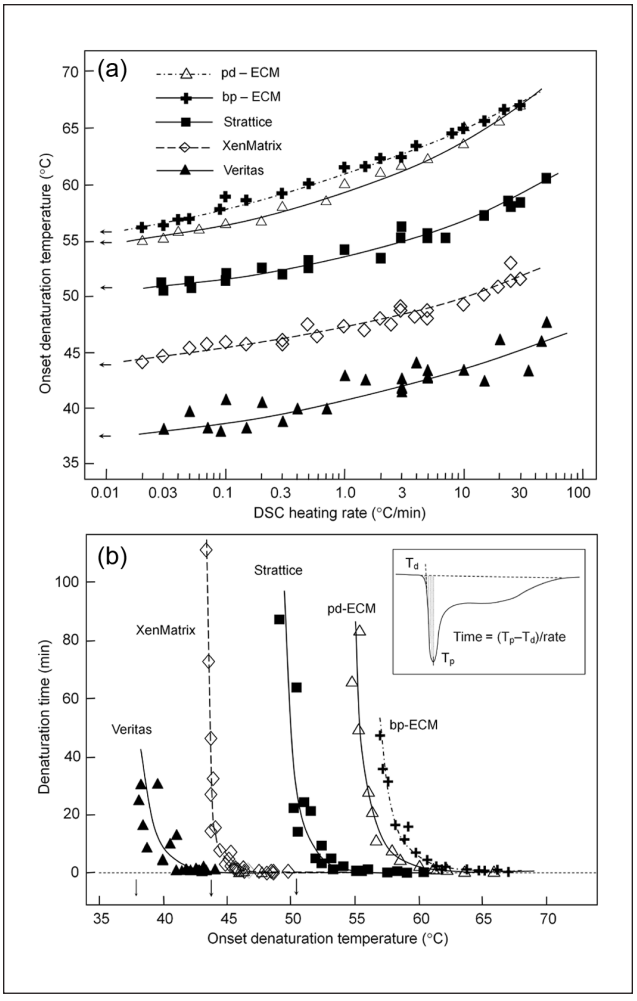

Figure 5. Effect of scan rates on bioscaffold denaturation temperatures: (a) Dependence of the onset denaturation temperatures (T_d) of bioscaffolds on the scan rate. Arrows indicate the extrapolated intrinsic T_d. (b) Thermal stability of bioscaffolds at different temperatures as measured by the duration of time needed to denature ~11% ECM (between the onset and peak temperature). The inset shows the method of calculating the duration of denaturation time.

ECM: extracellular matrix; pd-ECM: minimally processed porcine dermis ECM; bp-ECM: minimally processed bovine pericardium ECM; DSC: differential heating calorimetry.

To investigate further the changes in ECM properties after tissue processing, three scaffold products are analyzed with scan rates varying from 0.02°C/min to 50°C/min, which correspond to a change in time scale over three orders of magnitude (Figure 5(a)). The onset denaturation temperature of all ECM samples decreases as the scan rate is reduced, which is consistent with collagen denaturation as an irreversible, time-dependent kinetic process. Minimally processed native ECMs (i.e. porcine dermis ECM and bovine pericardium ECM) have higher onset denaturation temperatures than the derived commercial scaffolds, indicating that all tissue-processing technologies resulted in modifications that destabilize scaffolds (Figure 5(a)). There are significant differences among three commercial scaffolds. The intrinsic onset denaturation temperature (extrapolated to a scan rate of 0.01°C/min) is 55°C for the pd-ECM. The intrinsic onset denaturation temperature is reduced to 51°C and 44°C for Strattice and XenMatrix, respectively. Although the onset denaturation temperature of bovine pericardial ECM is higher than that of porcine dermal ECM, the derived Veritas has the lowest intrinsic onset denaturation temperature (38°C) (Figure 5(a)).

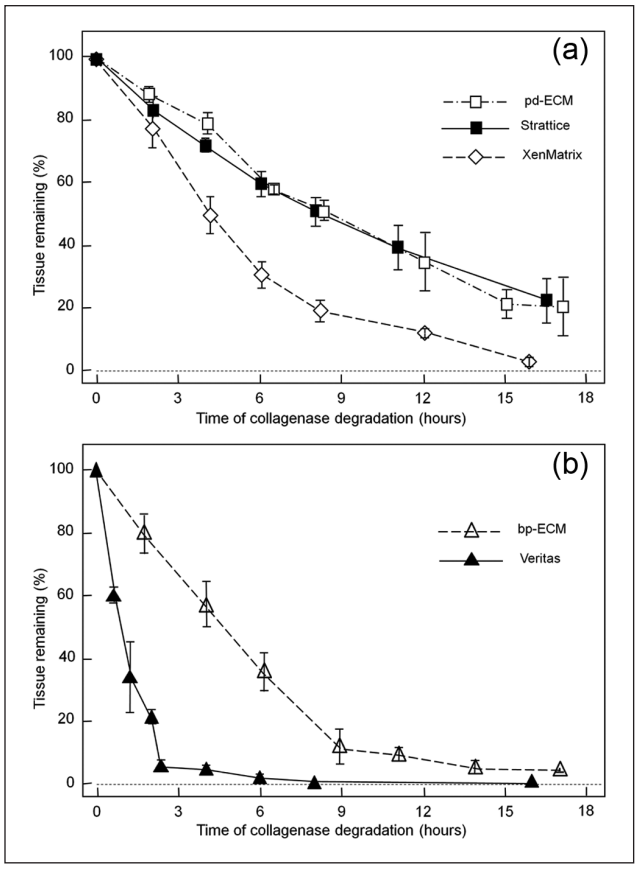

Figure 6. *Susceptibility of bioscaffolds to collagenase*. Susceptibility of three bioscaffolds to type I collagenase at 37°C: (a) Strattice and XenMatrix are compared with pd-ECM and (b) Veritas is compared with bp-ECM. Data are mean ± standard deviation. ECM: extracellular matrix; pd-ECM: minimally processed porcine dermis ECM; bp-ECM: minimally processed bovine pericardium ECM.

Process-caused modification and destabilization are also assessed by calculating the rate of protein denaturation at different onset temperatures (Figure 5(b)). The least stable ECM proteins denature between the onset denaturation temperature and the first peak temperature during a calorimetric measurement. This portion accounts for 11.1% ± 2.4% of the total ECM proteins, assuming that the differential enthalpy is proportional to the mass of denatured ECM proteins. The duration required to denature this portion of ECM proteins increased exponentially as temperature decreased. The ECM stability is in the order of bovine pericardial ECM > porcine dermal ECM > Strattice > XenMatrix > Veritas. The Veritas scaffold does not appear to be sufficiently stable at the human body temperature.

Differences in the susceptibility to collagenase

Figure 6 compares the susceptibility to type I collagenase between commercially available scaffolds and their respective minimally processed ECM materials. No significant difference is observed between Strattice scaffold and pd-ECM. Under the testing condition, the half-life is measured to be 8.9 ± 0.8 h (n = 6) and 8.5 ± 1.1 h (n = 5) for Strattice and pd-ECM, respectively. These values are similar to that of the fresh porcine skin material (8.9 ± 1.2 h, n = 7). The susceptibility of XenMatrix to type I collagenase is increased, with its half-life reduced to 4.8 ± 0.5 h (n = 3). The difference in the susceptibility to type I collagenase between Strattice and XenMatrix is statistically significant (p = 0.0001). The susceptibility of bovine pericardium ECM to type I collagenase is higher than porcine dermis ECM, possibly due to the fact that bovine pericardium is thinner and less dense than porcine dermis. The half-life of bp-ECM is 5.5 ± 0.6 h (n = 3). Veritas is the most susceptible to type I collagenase, with a half-life of 1.1 ± 0.3 h (n = 2), and about 80% is degraded within 2 h of incubation at 37°C.

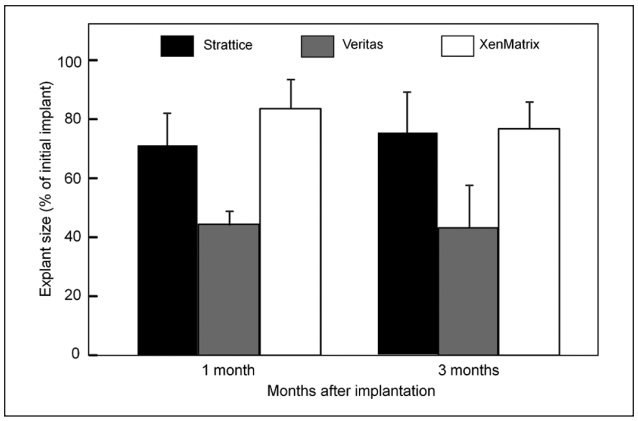

Figure 7. *Contraction of implanted bioscaffolds*. Changes of the size of implanted scaffolds after implantation in African green monkeys. All scaffold grafts were trimmed to 7 cm × 3 cm (i.e. 21 cm^2) at the time of implantation. Explanted grafts were smaller than the originally implanted grafts due to graft contraction and/or resorption. Data are mean ± standard deviation.

Differences in biological responses

In vivo evaluation using the abdominal wall repair primate model has demonstrated that three scaffold products exhibit distinctively different biological responses in soft tissue repair. All animals survived to the designated sacrifice date, with no herniation or bulging reported in any animals over the course of implantation. Gross evaluation of explanted grafts reveals no defect or graft hardening and shows good integration with adjacent host tissue for Strattice grafts. XenMatrix grafts show graft hardening and are less well integrated with surrounding host tissue at the 1-month and 3-month time points. Veritas-explanted grafts are much smaller than the pre-implants, indicating in vivo graft contraction. The size of Veritas grafts is reduced by ~60%, whereas the size of Strattice and XenMatrix grafts is reduced by ~20%–30% (Figure 7). Histological evaluation demonstrates that Strattice is rapidly repopulated with host

cells, and gradually remodeled over a period of 6 months, as indicated by new collagen deposition. Strattice results in minimal inflammatory response at the 1-month time point (Figure 8(a)–(c)). Veritas scaffold condensed and fused after 1-month of implantation into the primate, and lacked histological collagen structure as seen in the Veritas pre-implant (Figures 1 and 8(d)). Host cell infiltration of Veritas grafts is limited to peripheral at the 1-month time point, and thus, the most graft area remains acellular. At the 3- and 6-month time points, cell in-growth is stimulated. The implanted Veritas is difficult to be identified at the 3-month time point and appears to be completely absorbed with new collagen deposition observed at the implantation site. The implantation of Veritas results in moderate inflammation at the 1-month time point, and the inflammatory response lessens as the Veritas material is rapidly absorbed (Figure 8(e) and (f)). Implanted XenMatrix has demonstrated limited host cell in-growth at the 1-month time point, with host cells (including fibroblasts and macrophages) being able to get into the large pores only. Despite XenMatrix possessing the highest porosity among three scaffold products (Figures 1 and 8(g) to (i)), acellular areas are still observed at the 3- and 6-month time points (Figure 8(h) and (i)). Cell in-growth and new collagen deposition at the later time points occur at the slowly degraded and eroded scaffold areas. XenMatrix induces severe inflammation at all three time points, as demonstrated by the presence of numerous macrophages and foreign-body giant cells.

Figure 9 shows the elevation of systemic antibody (IgG) titer in animal serum in response to implanted scaffolds. Strattice results in the high IgG level initially (~100-fold increase), and the IgG titer gradually diminishes thereafter. Animals with implanted Veritas only had a small transient increase in the IgG titer during the first month, which returned to baseline level thereafter. XenMatrix also elevates the level of IgG titer in animals by ˜100-folds. Unlike Strattice, however, the high IgG level in animals with implanted XenMatrix remains unchanged for the entire experiment period (6 months), indicating a sustained humoral immune response.

Discussion and conclusion

This study aims to examine the relationship between ECM modifications by processing methods and the mechanisms of action in soft tissue repair and regeneration in vivo. Three commercially available scaffolds (Strattice, Veritas and XenMatrix) were selected for comparison for the following reasons. Tissue-processing methods for medical devices are validated to produce scaffolds of consistent quality. All three ECM scaffolds are non-cross-linked, packaged in the hydrated state, and terminally sterilized by e-beam irradiation. As a result, scaffold modifications are attributed mainly to tissue origin, process treatments for decellularization, and antigenicity reduction. The performance of these scaffold products in human patients has been documented,[12,38–42] and therefore, such a study could offer valuable biochemical and structural insights for the rational design of tissue engineering scaffolds for applications in human patients. In this study, we followed a previously described methodology that chooses in vitro ECM tests and in vivo animal models for evaluating the performance of ECM scaffolds.[43]

Three-dimensional structural properties of scaffolds are known to play critical roles in supporting new tissue formation via in situ cell repopulation and revascularization that ultimately lead to the remodeling of the ECM scaffold into a functional tissue. Processing methods alter scaffold structures differently (Figures 1 and 2). The Strattice process causes no or little visible structural modification, yielding an ECM scaffold with microscopic architecture and ultrastructural features similar to that of a native porcine dermis (supplemental Figure S1). In contrast, the XenMatrix process yields a substantially altered scaffold with few structural similarities to native dermal ECM. In vivo evaluation using the non-human primate model demonstrates a rapid fibroblast repopulation into Strattice ECM that is gradually remodeled (Figure 8(a)–(c)). Cell in-growth is limited in XenMatrix at the 1-month time point, despite the XenMatrix process being intentionally designed to loosen collagen network to increase the scaffold porosity for earlier cell repopulation,[33] and indeed, the XenMatrix scaffold has significantly more large pores than both native dermis and Strattice scaffold (Figures 1, 2 and supplemental Figure S1). The XenMatrix process results in the loss of fibrillar ultrastructural features of collagen bundles due to the condensation of collagen fibrils and fibers. Microscopic and ultrastructural features in scaffolds affect cell adhesion and migration.[44–46] The collagen structural damage by the XenMatrix process appears to outweigh the potential benefit of the increased scaffold porosity. Even at the 3- and 6-month time points (Figure 8(h) and (i)), acellular areas are still observed, and cell in-growth in XenMatrix is associated with slowly degraded areas. The Veritas process results in some matrix modifications, but fibrillar ultrastructures of collagen bundles are still preserved (Figures 1 and 2, supplemental Figure S1). Cell in-growth into the Veritas scaffold is limited to the periphery at the 1-month time point (Figure 8(d)) but is stimulated at 3- and 6-month time points. It is apparent that cell repopulation into Veritas is associated with the change in Veritas after implantation. Collagen bundles in the H&E histology of Veritas explanted at the 1-month time point were condensed (Figures 1 and 8(d)), which might have hindered cell repopulation. The implanted Veritas had largely degraded at the 3-month time point (Figure 8(e)).

Calorimetric analysis measures the changes in the thermophysical and thermochemical integrity of ECM scaffolds (e.g. structural destabilization, degradation, partial denaturation and cross-linking). The thermal denaturation profile of an ECM scaffold depends not only on the stability of its individual constituent proteins, but also on the

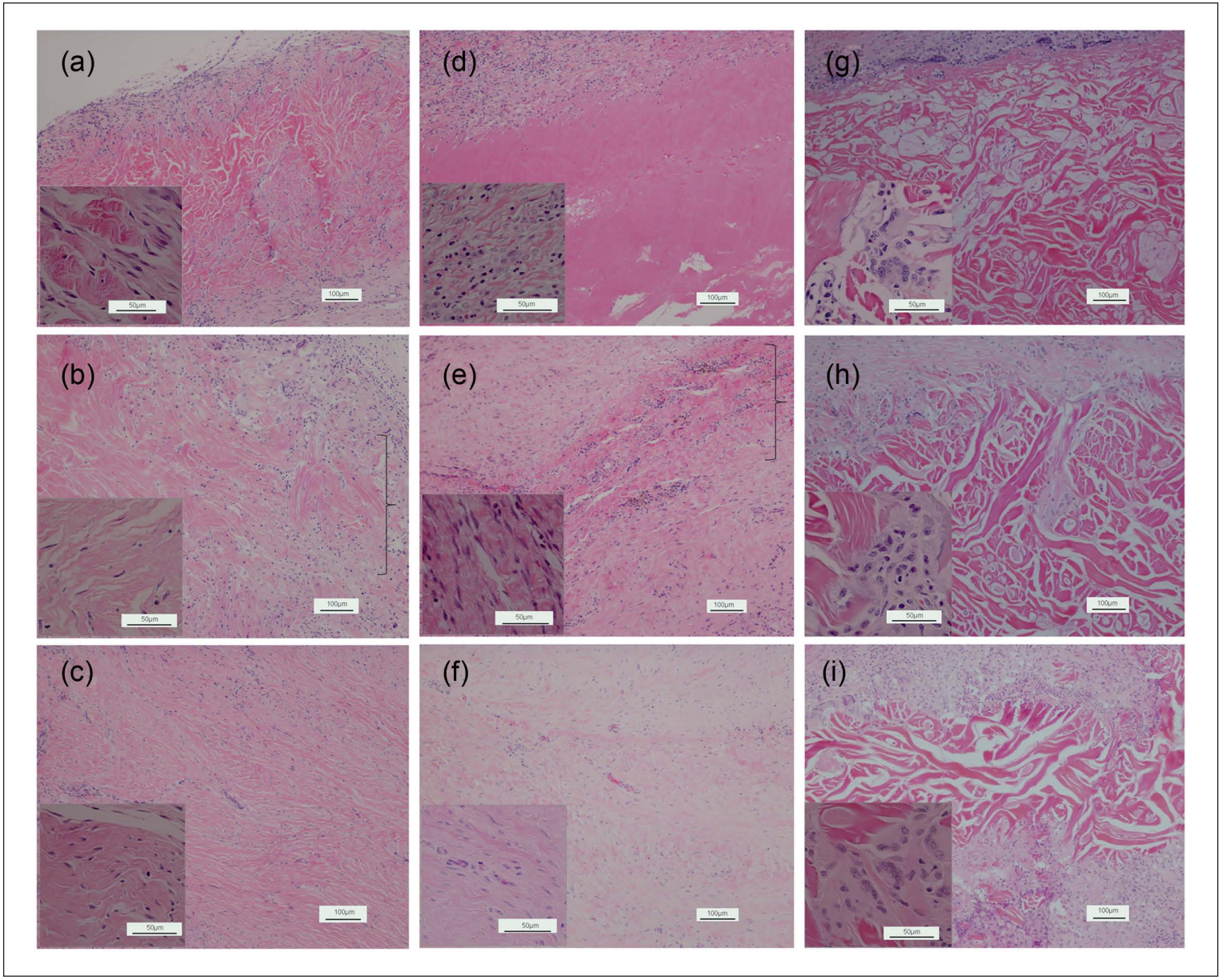

Figure 8. *Non-human primate cellular responses.* Histological micrographs (cross sections with hematoxylin and eosin stain) of explanted bioscaffolds after implantation in African green monkey for (a, d, and g) 1, (b, e, and h) 3 and (c, f, and i) 6 months. (a–c) Strattice, (d–f): Veritas, and (g–i): XenMatrix. The insets are representative micrographs at a high magnification showing the cell types in grafted materials. The bracket points to the implanted material.

supramolecular assembly of these proteins (i.e. fibrogenesis, fiber alignment, and deposition of non-collagen materials)—the process to form a stable tissue matrix with unstable molecules.[47,48] Calorimetric analysis shows that all three scaffold products are less stable than ECMs of their respective source tissues, demonstrating that processing treatments result in various degrees of ECM destabilization (Figure 4). The intrinsic matrix denaturation temperature is determined to be 51°C, 38°C, and 44°C for Strattice, Veritas, and XenMatrix, respectively (Figure 5). This intrinsic denaturation temperature is extrapolated to a scan rate of 0.01°C/min, corresponding to the duration of ~2 days for complete denaturation at the intrinsic denaturation temperature. The intrinsic denaturation temperature is 55°C for porcine dermal ECM. The Strattice process causes a moderate decrease by 4°C, whereas the XenMatrix process results in a decrease of 11°C. Nevertheless, XenMatrix is still stable at human body temperature. The Veritas scaffold with an intrinsic temperature of 38°C is not stable at human body temperature. It is conceivable that, upon implantation, the Veritas scaffold would denature spontaneously over a few days or weeks. We hypothesize that the instability of Veritas at body temperature could be the cause for structural condensation (Figure 8(d)) and limited cell in-growth at the peripheral region of the scaffold.

The decrease in thermal stability of scaffolds correlates with the increased vulnerability to enzyme degradation.[15,49,50] Significant differences exist in the susceptibility to collagenase among three scaffold products (Figure 6). Strattice has similar susceptibility to collagenase as fresh porcine dermis and minimally processed dermal ECM do. The susceptibility of the XenMatrix scaffold to collagenase is increased, as shown by the reduced half-life. The reduced half-life of the XenMatrix scaffold may be associated with the increased scaffold porosity by design as well as more severe matrix destabilization by tissue processing (as seen from calorimetric data). The Veritas process increases the susceptibility to collagenase even more than the XenMatrix process. The half-life of the Veritas scaffold to collagenase digestion is only ~20% of the half-life of the minimally processed bovine pericardial ECM. Not surprisingly, the Veritas scaffold is rapidly absorbed upon implantation in primates (Figures 7 and 8).

In vivo evaluation using the functional primate model shows that three scaffold products elicit different biological responses, have distinct mechanisms of action for tissue regeneration, and yield various outcomes of repairs. Strattice is well integrated into the host tissue through the mechanisms of cell repopulation, revascularization of the ECM scaffold, and a gradual remodeling process to new tissue matrix (Figure 8). This mechanism of action is characterized by minimal to mild inflammatory responses (Figure 8) and some humoral immune reactions at earlier time points after scaffold implantation (Figure 9). The process is similar to normal wound healing that involves an earlier inflammatory response phase, recruitment of different cell populations to the wound sites, and subsequent remodeling of damaged tissues. The coordinated

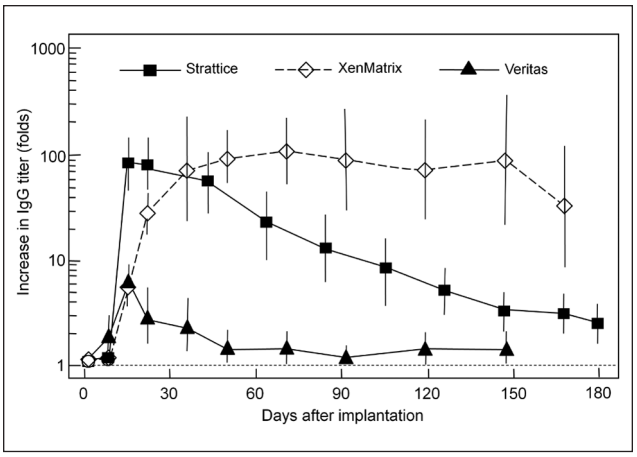

Figure 9. *Non-human primate immunological responses*. Elevation of systemic antibody (IgG) titer in the serum of animals after implantation of bioscaffolds over 6 months. The fold increase in antibody titer as compared with serum obtained prior to implantation was plotted on a logarithmic scale. Data are mean ± standard deviation.

structural and functional adaptations are likely driven by the positive interactions between the implanted ECM scaffold and repopulated host fibroblasts and other cell types.[51] Veritas demonstrates another mechanism of action, which is associated with moderate inflammation after implantation (Figure 8), transient immune reactions (Figure 9), and rapid scaffold resorption. As the implanted Veritas ECM degrades, cell ingrowth is stimulated, and the implanted scaffold is replaced with new collagen deposition. There is no remodeling of the implanted Veritas scaffold. The host responses to implanted XenMatrix grafts represent another different mechanism of action in soft tissue repair. XenMatrix elicits severe inflammation and sustained humoral immune reactions throughout the entire period of the experiment (6 months). The implanted scaffold shows hardening, poor integration with surrounding host tissue, and slow degradation. The pathology of graft hardening remains unclear. Graft hardening was documented previously for other biological scaffolds, including CollaMend (Davol, Cranston, RI), and Permacol (Tissue Science Laboratories, Aldershot, UK).[20] One common observation in this study and the earlier study[20] is the sustained presence of foreign-body giant cells and significant chronic inflammatory responses after implantation of these scaffolds into animals. Physiologically, hardening relates to the increased stiffness of tissue matrices, which could be caused by the formation of excessive fibrous tissue and/or encapsulation of implanted ECM grafts. There is evidence that the presence of foreign-body giant cells and chronic inflammation is accompanied by the formation of dense, poorly organized fibrous tissue for implanted scaffolds (CuffPatch, Permacol, and TissueMend) that is designed to degrade slowly in vivo.[19]

Functional tissue repair is affected by a variety of dynamic tissue-regenerative mechanisms and processes.

This study demonstrates that the manufacturing processes and tissue sources have significant impact on scaffold properties that may influence the mechanisms of action in tissue regeneration. The loss of biological and structural integrity of native ECMs is associated with severe inflammatory responses and sustained foreign-body reactions while hindering normal healing and tissue integration.

Supporting information

Figure S1. Micrographs (histological cross sections, hematoxylin-eosin stain) of unprocessed porcine dermis (**A**) and unprocessed bovine pericardium (**D**). Scanning electron micrographs (cross sections) show microscopic and ultrastructural features of unprocessed porcine dermis (**B**, **C**) and unprocessed bovine pericardium (**E**, **F**). Native extracellular matrices appear as tightly woven collagen fiber networks and have well-defined microscopic and ultrastructural characteristics, which could be altered by different tissue-processing methods.

Figure S2. De-convolution of the fresh porcine dermis calorimetric thermogram. The complex thermogram (**A**) are deconvoluted into individual peak components (**B**) using a mathematical software PeakFit (PeakFit 4.12, Systat Software, San Jose, CA), so that the changes of peak temperature and percentage area of individual components could be evaluated after tissue processing. Peak temperatures and their percent enthalpy values are mean ± standard deviation. Peak A disappears after cell lysis in water and a wash in phosphate-buffered saline, suggesting its origin of cellular proteins and loosely bounded ECM proteins. Minimally processed porcine dermis ECM retains Peak B and Peak C, without any change in their onset and peak temperatures.

Document S3. The detailed information about the animal welfare and care during the study.

The above data and information is available online with this article.

Acknowledgments

W.Q.S., M.S., and H.X. conceived and designed the experiments; W.Q.S., H.X., and J.L. performed the experiments; W.Q.S., H.X., and M.S. analyzed the data; W.Q.S., H.X., and J.L. contributed reagents/materials/analysis tools; and W.Q.S. wrote the article.

Declaration of conflicting interests

All authors are paid employees of LifeCell Corporation when the study was performed. The authors declare that there is no other conflict of interest.

Funding

The research was supported by LifeCell Corporation, and received received no other specific grant from any funding agency in the public, commercial, or not-for-profit sectors.

References

1. Parks WC, Wilson CL and Lopez-Boado YS. Matrix metalloproteinases as modulators of inflammation and innate immunity. *Nat Rev Immunol* 2004; 4: 617–629.
2. Rieder E, Kasimir MT, Silberhumer G, et al. Decellularization protocols of porcine heart valves differ importantly in efficiency of cell removal and susceptibility of the matrix to recellularization with human vascular cells. *J Thorac Cardiov Sur* 2004; 127: 399–405.
3. Badylak SF, Freytes DO and Gilbert TW. Extracellular matrix as a biologic scaffold material: structure and function. *Acta Biomater* 2009; 5: 1–13.
4. Hynes R. The extracellular matrix: not just pretty fibrils. *Science* 2009; 326: 1216–1219.
5. Wang W, Pan H, Murray K, et al. Matrix metalloproteinase-1 promotes muscle cell migration and differentiation. *Am J Pathol* 2009; 174: 541–549.
6. Burns JS, Kristiansen M, Kristensen LP, et al. Decellularized matrix from tumorigenic human mesenchymal stem cells promotes neovascularization with Galectin-1 dependent endothelial interaction. *PLoS One* 2011; 6(7): e221888.
7. Bellows CF, Alder A and Helton WS. Abdominal wall reconstruction using biological tissue grafts: present status and future opportunities. *Expert Rev Med Devic* 2006; 3: 657–675.
8. Ramshaw B and Bachman S. Surgical materials for ventral hernia repair—biological mesh (part 2 of 3). *Gen Surg News* 2007; 34(2): 1–15.
9. Deeken CR, Eliason BJ, Pichert MD, et al. Differentiation of biological scaffold materials through physicomechanical, thermal and enzymatic degradation techniques. *Ann Surg* 2012; 255: 595–604.
10. Millennium Research Group (MRG). US Markets for soft tissue repair devices 2012, October 2011.
11. Macchiarini P, Jungebluth P, Go T, et al. Clinical transplantation of a tissue-engineered airway. *Lancet* 2008; 372: 2023–2030.
12. Kaplan KM, Chopra KK, Feiner JF, et al. Chest wall reconstruction with Strattice in an immunosuppressed patient. *Eplasty* 2011; 11: 479–485.
13. Badylak SF, Weiss DJ, Caplan A, et al. Engineered whole organs and complex tissues. *Lancet* 2012; 379: 943–952.
14. Gouk SS, Lim TM, Teoh SH, et al. Alterations of human acellular tissue matrix by gamma irradiation: histology, biomechanical property, stability, in vitro cell repopulation and remodeling. *J Biomed Mater Res B* 2008; 84B: 205–217.
15. Sun WQ and Leung P. Calorimetric study of extracellular tissue matrix degradation and instability after gamma irradiation. *Acta Biomater* 2008; 4: 817–826.
16. Reing JE, Brown BN, Daly KA, et al. The effects of processing methods upon mechanical and biologic properties of porcine dermal extracellular matrix scaffolds. *Biomaterials* 2010; 31: 8626–8633.
17. Brown BN, Londono R, Tottey S, et al. Macrophage phenotype as a predictor of constructive remodeling following the implantation of biologically derived surgical mesh materials. *Acta Biomater* 2012; 8: 978–987.
18. Daly KA, Liu S, Agrawal V, et al. Damage associated molecular patterns within xenogeneic biologic scaffolds and their effects on host remodeling. *Biomaterials* 2012; 33: 91–101.

19. Valentin JE, Badylak JS, McCabe GP, et al. Extracellular matrix bioscaffolds for orthopaedic applications. A comparative histologic study. *J Bone Joint Surg Am* 2006; 88: 2673–2686.
20. Sandor M, Xu H, Connor J, et al. Host response to implanted porcine-derived biologic materials in a primate model of abdominal wall repair. *Tissue Eng Pt A* 2008; 14: 2021–2031.
21. Xu H, Sandor M, Qi S, et al. Host response to human acellular dermal matrix transplantation in a primate model of abdominal wall repair. *Tissue Eng Pt A* 2008; 14: 2009–2019.
22. Xu H, Wan H, Zuo W, et al. A porcine-derived acellular dermal scaffold that supports soft tissue regeneration: removal of terminal galactose-alpha-(1,3)-galactose and retention of matrix structure. *Tissue Eng Pt A* 2009; 15: 1807–1819.
23. Butler CE, Burns N, Campbell KT, et al. Comparison of cross-linked and non-cross-linked porcine acellular dermal matrices for ventral hernia repair. *J Am Coll Surgeons* 2010; 211: 368–376.
24. Melman L, Jenkins ED, Hamilton NA, et al. Early biocompatibility of crosslinked and non-crosslinked biologic meshes in a porcine model of ventral hernia repair. *Hernia* 2011; 15: 157–164.
25. Shah BC, Tiwari MM, Goede MR, et al. Not all biologics are equal. *Hernia* 2011; 15: 165–171.
26. Campbell KT, Burns N, Rios CN, et al. Human versus non-cross-linked porcine acellular dermal matrix used for ventral hernia repair: comparison of in vivo fibrovascular remodeling and mechanical repair strength. *Plast Reconstr Surg* 2011; 127: 2321–2332.
27. Deeken CR, Melman L, Jenkins ED, et al. Histologic and biomechanical evaluation of crosslinked and non-crosslinked biologic meshes in a porcine model of ventral incisional hernia repair. *J Am Coll Surgeons* 2011; 212: 880–888.
28. Keane TJ, Londono R, Turner NJ, et al. Consequences of ineffective decellularization of biologic scaffolds on the host response. *Biomaterials* 2012; 33: 1771–1781.
29. Connor J, McQuillan D, Sandor M, et al. Retention of structural and biochemical integrity in a biological mesh supports tissue remodeling in a primate abdominal wall model. *Regen Med* 2009; 4: 185–195.
30. Oray BN. Veritas® collagen matrix safety studies, Synovis Surgical Innovations, White paper 88004D 04/05, 2001, http://www.synovissurgical.com/pdfs/88004D_Oray_paper.pdf (2011, accessed 15 October 2012).
31. Oray BN, Lambert A, Wonsetler R, et al. Physical and biochemical characterization of a novel non-crosslinked, propylene-oxide treated acellular collagen matrix: comparison with solvent-extracted and freeze-dried cadaveric fascia lata. In: *17th Annual meeting of the society for urology and engineering*, Orlando, FL, 25 May 2002.
32. Mooradian DL, Lambert A, Wonsetler R, et al. Residual DNA in biological sling materials: a comparison between PO-treated bovine pericardium, human dermis, solvent-extracted and freeze-dried cadaveric fascia lata. In: *17th Annual meeting of the society for urology and engineering*, Orlando, FL, 25 May 2002.
33. Brennen Medical. XenMatrix® acellular collagen matrix for reconstructive, soft tissue and hernia repairs (product brochure), 100566, E-11/08, 2008.
34. Klein D and Katzner LD. *Biocompatible tissue for therapeutic use and method of making same*. US Patent 6,933,103 B1, 2005.
35. Chao J and Koumanis D. *Veritas collagen matrix for breast reconstruction: veritas for tissue expansion—surgical guidance*. 88154A 10/08, 2008. St Paul, MN: Synovis Surgical.
36. Wicker HS. *Management of abdominal wall defects in contaminated and dirty wounds (clinical review)*. 880931A 01/08, 2008. St Paul, MN: Synovis Surgical.
37. Canadian Agency for Drugs and Technologies in Health (CADTH). Biological mesh: a review of clinical indications, clinical effectiveness, cost-effectiveness, and clinical practice guidelines. CADTH, 8 November 2010.
38. Agarwala N and Cohn A. Experiences with a xenograft (acellular bovine collagen matrix) in gynecologic fistula repairs. *J Minim Invasive Gynecol* 2006; 13: 483–485.
39. Connolly RJ. Evaluation of a unique bovine collagen matrix for soft tissue repair and reinforcement. *Int Urogynecol J Pel* 2006; 17(Suppl. 1): S44–S47.
40. Guerette N, Aguirre O, VanDrie DM, et al. Multi-center, randomized prospective trial comparing anterior colporrhaphy alone to bovine pericardium collagen matrix graft (Veritas) reinforced anterior colporrhaphy: 12 month analysis. *Int Urogynecol J* 2006; 17: S57–S100.
41. Croston JK. Clinical experience with XenMatrix graft. *White paper MMCR 6 of Davol Inc*, http://www.davol.com/default/assets/File/Product_Files/XenMatrix_Clin_SurgMono_Final.pdf (2009, accessed on 15 October 15 2012).
42. Netscher DT, Izaddoost S and Sandvall B. Complications, pitfalls, and outcomes after chest wall reconstruction. *Semin Plast Surg* 2011; 25: 86–97.
43. Qiu QQ, Sun WQ and Connor J. Sterilization of biomaterials of synthetic and biological origin. In: Ducheyne P, Healy KE, Hutmacher DW, et al. (eds) *Comprehensive biomaterials*, vol. 4. Amsterdam: Elsevier, 2011, pp. 127–144.
44. Brown B, Lindberg K, Reing J, et al. The basement membrane component of biologic scaffolds derived from extracellular matrix. *Tissue Eng* 2006; 12: 519–526.
45. Sellaro TL, Ravindra AK, Stolz DB, et al. Maintenance of hepatic sinusoidal endothelial cell phenotype in vitro using organ-specific extracellular matrix scaffolds. *Tissue Eng* 2007; 13: 2301–2310.
46. Gong J, Sagiv O, Cai H, et al. Effects of extracellular matrix and neighboring cells on induction of human embryonic stem cells into retinal or retinal pigment epithelial progenitors. *Exp Eye Res* 2008; 86: 957–965.
47. Leikina E, Mertts MV, Kuznetsova N, et al. Type I collagen is thermally unstable at body temperature. *P Natl Acad Sci U S A* 2002; 99: 1314–1318.
48. Persikov AV and Brodsky B. Unstable molecules form stable tissues. *P Natl Acad Sci U S A* 2002; 99: 1101–1103.
49. Danielsen CC. Age-related thermal stability and susceptibility to proteolysis of rat bone collagen. *Biochem J* 1990; 272: 697–701.
50. Sun WQ and Gouk SS. Aging of a regenerative biologic scaffold (AlloDerm native tissue matrix) during storage at elevated humidity and temperature. *Tissue Eng Pt C: Meth* 2009; 15: 23–31.
51. Harper JR and McQuillan DJ. Extracellular wound matrices: a novel regenerative tissue matrix (RTM) technology for connective tissue reconstruction. *Wounds* 2007; 19: 163–168.